Article

Charged Hybrid Microstructures in Transparent Thin-Film ITO Traps: Localization and Optical Control

Dmitrii Shcherbinin *[ID], Vadim Rybin [ID], Semyon Rudyi [ID], Aliaksei Dubavik, Sergei Cherevkov [ID], Yuri Rozhdestvensky [ID] and Andrei Ivanov [ID]

International Research and Educational Centre for Physics of Nanostructures, ITMO University, Kronverksky Prospekt 49, Bldg. A, St. Petersburg 197101, Russia
* Correspondence: shcherbinin.dmitrij@gmail.com

Abstract: In the present study, we propose a new transparent thin-film ITO surface radio-frequency (RF) trap. Charged hybrid microstructures were localized in the developed ITO trap. We show, analytically and experimentally, that the position of the localization zones in the trapped hybrid structure are stable. The transfer of charged particles between localization zones was studied under the action of gravity-compensating laser radiation. We highlight the advantages of transparent thin-film ITO traps to investigate and manipulate charged particles.

Keywords: thin films; indium tin oxide; surface ion trap; optomechanics; double-well trap; microstructures

1. Introduction

Ion traps are a versatile tool for the retaining and manipulating of charged particles. Trapped particles levitate in a radio-frequency (RF) electrical field and become isolated in space. Different RF trap configurations allow the localization of charged particles, varying from atomic ions to microparticles [1–3]. Different types of measurements can be conducted with RF traps. Ion trapping techniques have been adopted for the following: mass spectrometry [4,5], quantum computing and quantum simulating [6–9], plasma research [10,11], and the studying, and characterization, of micro- and nano-particles [11–13]. RF traps have become useful tools to research the spectral and physical properties of luminescent particles [14–16].

Different applications require different configurations of RF traps, from quadrupole traps [2,17] to surface traps with integrated fiber optics [18,19]. However, due to the geometry of electrodes most RF traps are challenged by limited optical access and low optical collection efficiency [7,19,20]. Recently, the collection efficiency was enhanced with the use of hemispherical mirrors and an improved design of trap electrodes [21]. We propose that the use of surface traps with transparent conducting electrodes would be a solution. This configuration allows full optical access to a localized object from any angle and supports direct coupling with optical equipment.

There are only a few materials that feature both high transparency in the visible range and near-metallic conductivity. Nowadays, transparent conductive oxides, such as graphene, as well as a composite structure with ultrathin metallic films, are promising candidates for the preparation of transparent electrodes [22–25]. As one of the most studied materials, we suggest using indium tin oxide (ITO) for RF trap transparent electrodes. ITO is an *n*-type degenerated wide-gap semiconductor with high transmittance in visible region and near-metallic conductivity. Usually, ITO thin-film structures are deposited by well-known magnetron sputtering techniques [26–29]. The variation of sputtering conditions (working gas pressure and mixture, sputtering power, substrate temperature, post annealing) may lead to changes in conductivity, transparency, surface morphology, and optical band gap, as well as the refractive indices of the deposited films [26–32]. The

application value of ITO thin films has been proven in liquid–crystal cells, photovoltaic cells, and gas sensors [33–36].

In the present study, we propose a new type of transparent thin-film ITO surface RF trap for the localization and manipulation of charged particles [19]. This type of RF trap provides full optical access to a localized particle, including direct laser illumination. To highlight the advantages of the fully transparent trap, we developed a double-well (DW) trap design. It has been shown that, in RF traps with DW potential, the trapped particle positions are extremely sensitive to all system parameters [37–40]. The developed trap supports particle localization in two stable zones isolated in space. Control of the trapped particle position can be implemented via switching between double-well and single-well (SW) regimes with only one stable localization zone. The proposed analytical model shows that DW to SW regime transition is possible in the case of trapped particles' gravity force compensations. We propose to compensate the particle's gravity with a laser beam, where the wave vector is directed in an opposite direction to that of the particle's gravity vector. Our experimental study revealed the opportunity to manipulate the levitating particle position with a gravity-compensating laser.

2. Materials and Methods

Transparent thin-film ITO electrodes were deposited by magnetron sputtering of an indium-tin alloy target (90 wt% In and 10 wt% Sn). Thin films were deposited on transparent glass substrates through the contact mask determining the geometry of electrodes (Figure 1a). A mixture of argon and oxygen in a ratio of 3:1 was used as the working gas medium. The conductivity and transmission of ITO thin films can be varied by changing the deposition rate. The full process is discussed in detail in [31]. In the studied trap, ITO electrodes consisted of a 170 nm thick conductive layer, coated with a 30 nm thick ITO insulating transparent film (with excess oxygen content) deposited in the same technological process. Layer thickness was controlled by quartz scales during the deposition process. To improve adhesion, the deposited layers were annealed in the atmosphere at a temperature of 400 °C for 20 min. The conductivity of the uninsulated ITO electrodes was 100 Ohm/square.
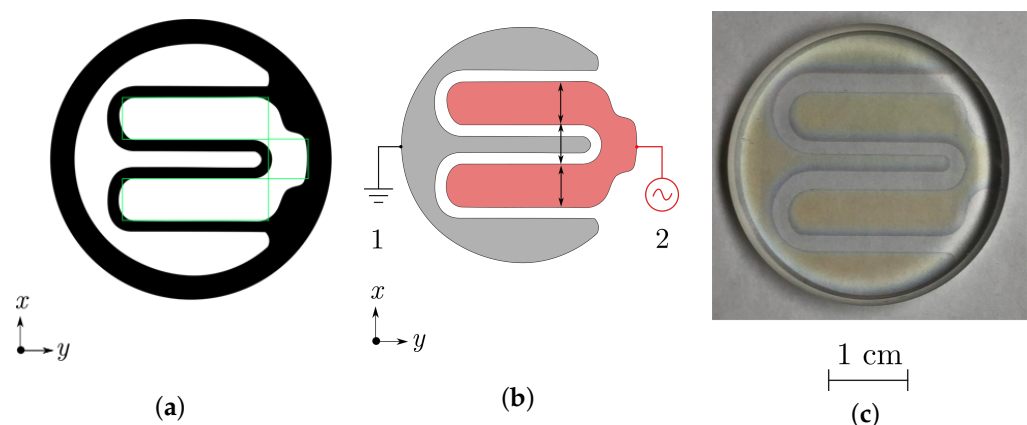

Figure 1. (**a**) Contact mask determining ITO-trap electrodes' geometry. The rectangular approximation is marked in green (Appendix A). (**b**) Principal scheme of double-well ITO surface trap. Gray (1) and red (2) indicate grounded and RF electrodes. (**c**) Photograph of the prepared ITO trap.

A surface RF trap can be represented as a set of several electrodes on a dielectric substrate. The simplest surface trap consists of five rectangular electrodes ("5-wire" design [41]). Such an electrode design provides a single quasi-equilibrium point. A possible solution for implementing SW and DW modes is to use asymmetric electrodes. In the present work, we propose a system of U-shaped and W-shaped electrodes for DW potential formation. Figure 1b represents the principal scheme for the DW surface RF trap, where gray and red indicate the grounded W-shaped and RF U-shaped electrodes, respectively.

The width of the U-shaped electrodes and the distance between them was $a = 6$ mm (marked with black arrows in Figure 1). A photograph of the prepared ITO trap is provided in Figure 1c. The electrodes' geometry was designed so as to obtain a double-well effective potential in the YZ-plane for the studied microspheres. We propose using the RF trap with DW potential, since, in such traps, the equilibrium points of particles strongly depend on all the system parameters [37–40]. The principles of DW potential formation for the proposed electrode geometry, as well as for effective potential simulation for SW and DW localization regimes, are discussed in Appendix A.

In the configuration with fully transparent surface electrodes (Figure 1b), it is possible to use intense laser radiation to achieve localized particle manipulation. Transparent ITO electrodes and a glass substrate allow UV laser radiation to propagate through the entire trap. In the present study, we used UV laser beams with the wave vector directed opposite to the particle's gravity force vector (Figure 2). Such an approach provides an opportunity to compensate the localized particle's gravity by the scattering force and to control the positions of the trapped particles.
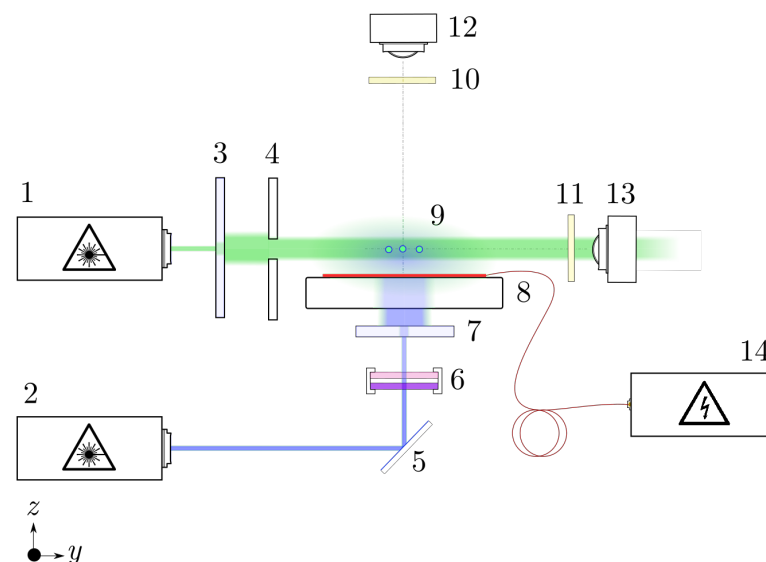

Figure 2. Principal scheme of the experimental setup with thin-film ITO trap: 1—535 nm laser source; 2—405 nm UV lase source; 3, 7—beam expander; 4—aperture; 5—mirror; 6—UV-attenuation filter system; 8—ITO surface trap; 9—localized charged particles; 10, 11—UV-filters; 12, 13—cameras; 14—trap's power supply.

To conduct experimental research, we prepared the optical setup shown in Figure 2. The setup consists of an ITO trap, 535 and 405 nm lasers, and two high-speed digital cameras. The green laser beam directed parallel to the trap's surface was used to illuminate trapped particles. We used a beam expander and aperture to adjust the green laser light to the whole localization area above the trap's surface. Two digital cameras were used to track the motion of the trapped particles. The first camera was directed perpendicularly to the trap from above to film the motion of the particles in the XY-plane. The second camera was directed parallel to the trap's surface in the YZ-plane. To avoid registration of scattered UV light from the trap electrodes and substrate, UV filters were used. The neutral filter was used to attenuate the UV laser intensity.

As an object of localization we used pre-synthesized $CaCO_3$-Fe_3O_4-$AgInS_2$/ZnS microspheres with diameter 3.5–4 μm [42]. The experimental conditions were the following: an U-shaped electrode, the width and distance between them equaling $a = 6$ mm (Figure 1); RF voltage amplitude on the electrode of $V = 2750$ V; frequency of RF voltage of $\omega = 100$ Hz. The $CaCO_3$ microspheres were introduced by a pneumatic injection system.

According to published data, the approximate charge of a single microparticle of the same order of size falls within the interval $6.9 \times 10^3 - 8.4 \times 10^3$ elementary charge [43].

3. Results and Discussion

Here, we propose the method of controlling the positions of charged particles by compensating for gravity using a light scattering force. We would like to highlight that optical compensation of gravity in surface traps is only possible with the use of fully transparent thin-film electrodes.

The localization of charged particles near the surface of the proposed trap is caused by the interaction of the charged particles with the RF electrical field on the thin-film ITO electrodes. The spatial position of a trapped particle above the electrode's surface is determined by the superposition of all the forces acting on levitating particles, such as the electrical and gravitational forces. Thus, changing the ratio of these forces, or introducing a new one, can lead to shift in the particle position. In this way, the localization process can be sufficiently modified in the presence of the acting scattering force originating from the laser beam.

To account for all the forces acting on the levitating particle, we propose using effective potential formalism, which is sufficiently discussed in the following works [44,45]. Thus, we propose describing the localization process in terms of effective potential. To prove the proposed optical position control concept, we carried out a calculation of effective potential spatial distribution in the presence and absence of the light scattering force, corresponding to compensated and uncompensated gravity force cases. The effective potential can be represented as the superposition of an average kinetic energy of fast oscillation and the potential energy of a dynamical system [44,45]. The description of the model used is in Appendix A. Notably, every particle is characterized by its own effective potential, which is determined by its own mass, size, and charge and the superposition of the external forces. Thus, the same setup provides different effective potential distribution for particles with various sizes, masses and charges. The full discussion of effective potential formation depending on the characteristics mentioned above is provided in Appendix A. Further, we discuss an effective potential map for the single $CaCO_3$ microparticle with mass $m = 9.1 \times 10^{-14}$ kg, size $2r = 4$ μm, $e = 8.4 \times 10^3$ elementary charge. We take into account the following RF field parameters $V = 2750$ V, $\omega = 100$ Hz, the trap geometry parameter $a = 6$ mm.

The map of effective potential distribution over the surface trap in the YZ-plane for the studied cases is shown in Figure 3. The colors of the given maps represent the effective potential normalized values, while the black lines are equipotential lines. Figure 3a corresponds to the case of the localization of $CaCO_3$ spheres above the surface of the studied ITO trap in the absence of the light scattering force. We can see two independent potential minima marked with asterisks on the map corresponding to two independent localization zones. This means that charged $CaCO_3$ particles can stably localize in two independent isolated areas above the surface of the studied ITO trap (DW regime). In the presence of light, with the wave vector directed opposite to the gravity force vector, the superposition of the forces along the Z-axis changes. Figure 3b presents the map of the effective potential in the case when the scattering force fully compensates the gravitational force. As seen, only one potential minimum corresponds to one stable localization zone. In this case, localization of the studied microspheres occurred only in one region (SW). We can conclude that compensation of the levitating charged particle gravity by the scattering force leads to transition from the DW regime to the SW regime.
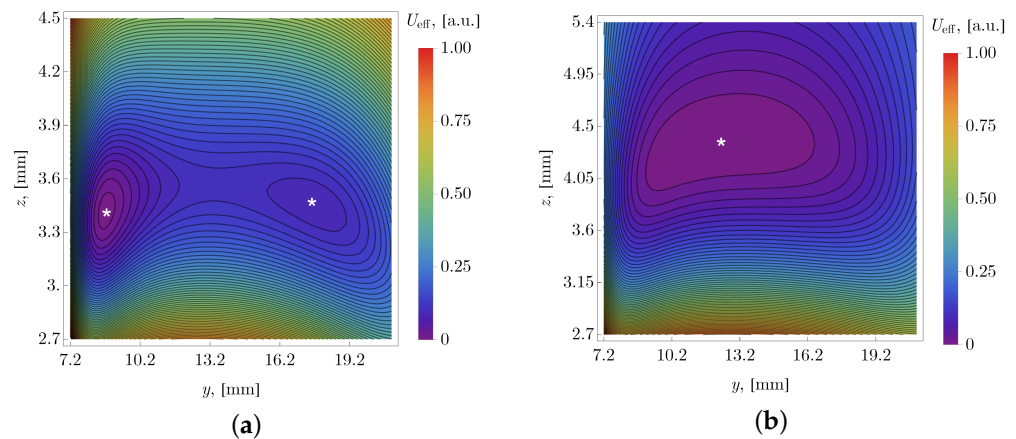
Figure 3. Effective potential distribution for the case of uncompensated gravity (**a**), and full gravity compensation (**b**). White asterisk indicates the potential minima coordinates.

To verify the simulation results, we conducted an experiment with the setup shown in Figure 2. We investigated the spatial distribution of $CaCO_3$ microspheres in the electric field of an ITO trap with and without UV light action. Photographs of the charged levitating $CaCO_3$ particles over the surface of the studied trap were taken in the YZ-plane, and are shown in Figure 4. The particles' oscillation amplitudes during the localization process was much higher than its actual size. Thus, Figure 4 represents the particles' oscillation trajectories, rather than the actual particles.
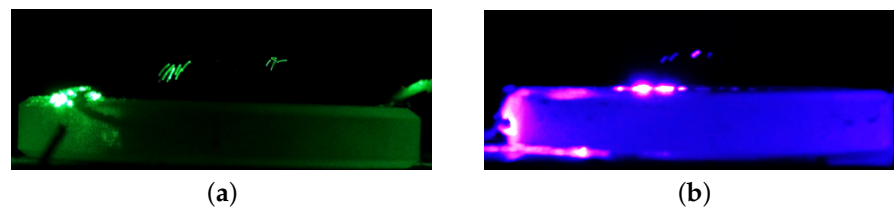

Figure 4. Trapped hybrid microstructures levitate above the ITO trap's surface. (**a**) Two groups of particles were located in two isolated localization zones while their gravity was not compensated. (**b**) One group of particles was located in a single localization zone while its gravity was compensated with the UV laser.

Figure 4a presents two independent groups of levitating particles over the surface of the ITO trap. As can be observed, without gravity compensation, the DW regime was realized as predicted by the analytical estimation (Figure 3). The photographs of charged levitating particles after the UV light was switched on is represented in Figure 4b. Only one broad regime of localization was observed, which agrees well with the proposed model. During the experimental procedure, we adjusted the intensity of UV light by means of a filter (Figure 2), since lower intensity light did not provide enough scattering force value, and high intensity light led to delocalization of particles (i.e. particles left the localization zone). Generally speaking, the relation between the switching from DW to SW regimes in response to laser intensity can be used to develop a new way of estimating such trapped particle characteristics as mass, charge, and size.

We studied a set of experimental video footage of charged levitating particle positions along the Y-axis in the presence and absence of a light scattering force. The coordinates of each independent particle were obtained by the computer vision method. In each frame, we tracked bright pixels, which correspond to light scattered on levitating particles. The number of bright pixels counted along the Y-axis were collected for 5 s periods for UV-on and UV-off laser modes. The number of counts in each point along the Y-axis corresponded to the particle detection probability at the same point.

Figure 5 represents the total counts of bright pixels over the experiment. The red curve in Figure 5 corresponds to the $CaCO_3$ microspheres' detection frequency on the Y

coordinate in the DW regime. The blue curve corresponds to the CaCO$_3$ microspheres' detection frequency on the Y coordinate in the SW regime after the gravity-compensating UV-laser was switched on. The results of bright pixel detection processing agreed well with the proposed model of the effective potential .
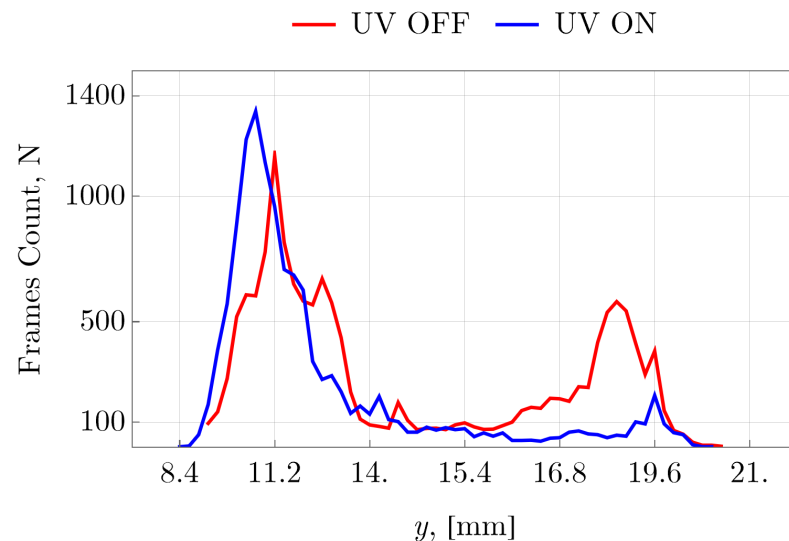

Figure 5. Particles' distribution in the surface ITO trap in the gravity-uncompensated regime (marked in red) and optical gravity compensation regime (marked in blue); accumulation was carried out for 600 s.

At the same time, in our experiment there was a small probability of particle detection between stable localization zones in the DW regime, Figure 5. Likewise, one can see that, even after switching on the UV laser, a small second localization zone still remained. Both these observations were associated with transient effects when the UV laser was switched on and stochastic motions of the particle trapped under the atmospheric conditions.

Discrepancy between the potential minima coordinates in the simulation results, in Figure 3, and the statistical experimental data, in Figure 5, can be explained by the fact that the simulations were performed with certain values of charge, mass and size for a single CaCO$_3$ microsphere. The real ensemble of CaCO$_3$ microspheres consists of particles with some parameter dispersion. The deviation of mass to charge ratio leads to shift in the potential minima coordinates in the developed trap (see Appendix A).

4. Conclusions

In the present study, we developed a new type of surface RF trap, which provides full optical access to the trapped charged particle. The advantage of full optical access was achieved by means of transparent conducting ITO thin film acting as the trap's electrodes. The proposed approach supports charged microparticle levitation above the trap's surface and provides an opportunity to compensate the particle's gravity with an optical scatterings force.

To observe the gravity compensation effect most clearly, we designed a DW surface RF trap, where the trapped particle position was highly sensitive to the particle parameters, localization conditions and external influences. The numerical simulation of the effective potential for the proposed trap geometry showed two separate stable localization zones for charged microparticles. By having the scattering force directed opposite to the particle's gravity in the simulation the confluence of two potential minima into one resulted.

We prepared an RF trap with thin-film ITO electrodes deposited on a glass substrate using the magnetrone sputtering technique. Fully transparent conducting electrodes supported propagation of the laser beam with the wave vector directed opposite the particle's gravity vector. It was shown that without a gravity-compensating laser beam, charged

CaCO$_3$ microspheres grouped in two separate localization zones above the ITO electrodes. After switching on the gravity-compensating laser, all trapped particles relocated to the single stable localization zone. The experimental observations agreed well with the numeric simulation results.

The proposed surface ITO RF trap opens up a new way of conducting optical experiments with trapped charged particles. Full optical access to the trapped particle can improve the optical collection efficiency of a trapped object and allow RF trap deposition directly onto optical surfaces and equipment. This work presented the concept of transparent RF traps and its practical implementation. We would like to highlight that the shape and material selected for the trap electrode can be optimized in accordance with a specific task.

Abbreviations

The following abbreviations are used in this manuscript:

RF	Radio-frequency
ITO	Indium tin oxide
UV	Ultraviolet
SW	Single-well
DW	Double-well

Appendix A. ITO Double Well Trap Model

Effective potential minima coordinates of the proposed ITO RF trap are strictly related to the trap's voltage parameters and gravity-compensating laser parameters, as well as to the trapped particle parameters. We assume that the three main forces acting on a levitating charged particle are the electrical force from the trap electrodes, gravitational force, and light scattering force.

To describe trapped particle–electric field interaction it is convenient to consider electrical potential distribution above the trap's U-shaped electrode (Figure 1). An approximation of the electrode's shape was performed with a well-known rectangular fitting [46]. Then, electrical potential distribution takes the following form

$$U(x,y,z) = V \cos(\omega t) \sum_{i=1}^{3} \frac{1}{2\pi} \left[\tan^{-1} \left(\frac{(x_{1i} - x)(y_{1i} - y)}{z\sqrt{(x_{1i} - x)^2 + (y_{1i} - y)^2 + z^2}} \right) - \right. \tag{A1}$$

$$- \tan^{-1} \left(\frac{(x_{1i} - x)(y_{2i} - y)}{z\sqrt{(x_{1i} - x)^2 + (y_{2i} - y)^2 + z^2}} \right) -$$

$$- \tan^{-1} \left(\frac{(x_{2i} - x)(y_{1i} - y)}{z\sqrt{(x_{2i} - x)^2 + (y_{1i} - y)^2 + z^2}} \right) +$$

$$\left. + \tan^{-1} \left(\frac{(x_{2i} - x)(y_{2i} - y)}{z\sqrt{(x_{2i} - x)^2 + (y_{2i} - y)^2 + z^2}} \right) \right] =$$

$$= V \cos(\omega t) f_V(x,y,z), \tag{A2}$$

where V, ω is amplitude and frequency of AC voltage on the U-shaped electrode, $i = 1 \ldots 3$ is an increment of the electrode's segment, x_{1i}, y_{1i}, x_{2i}, y_{2i} are rectangle apex coordinates (marked in green on Figure 1a).

Particle–light interaction can be accounted for as the light scattering force in the following form

$$F_z = \mu P \frac{r^2}{r_0^2} Q_{pr}, \tag{A3}$$

where $\mu = 3.33 \times 10^{-12}$, P is power of the laser source, r is the particle radius, r_0 is the laser beam radius, Q_{pr} is the radiation pressure efficiency [47].

Complementing the Euler–Lagrange equation for a charged particle in the trap's electric potential with its gravitational force and a non-conservative light scattering force along the Z-axis, we can obtain the particle's equation of motion. The particle acceleration projection on the Z-axis can be written as

$$\ddot{\tilde{z}} = -\frac{\partial f_V(\tilde{x}, \tilde{y}, \tilde{z})}{\partial \tilde{z}} \frac{eV \cos(\omega t)}{ma^2} + \left(\frac{g}{a} - \frac{\mu P}{ma} \frac{r^2}{r_0^2} Q_{pr} \right), \tag{A4}$$

where $\tilde{z} = z/a$, $\tilde{x} = x/a$, $\tilde{y} = y/a$, a is the electrode width. Using dimensionless time substitution $\tau = \omega t/2$ we obtain the final form

$$\ddot{\tilde{z}} = -\frac{\partial f_V(\tilde{x}, \tilde{y}, \tilde{z})}{\partial \tilde{z}} 2q \cos(2\tau) + \alpha, \tag{A5}$$

where $q = 2eV/(ma^2\omega^2)$ is the electrical field-charged particle interaction parameter; $\alpha = 4g/\omega a - (4\mu r^2 P Q_{pr})/(ma\omega^2 r_0^2) = \alpha_0 - \alpha_1$; α_0 is normalized acceleration parameter, α_1 is light-particle interaction parameter. The accelerations in the XY-coordinates take a similar form to the corresponding partial derivative and the inhomogeneous term α. Notably, the α_0 term is defined by the surface trap's, but not the particle's trap's, parameters. As α_0 is predetermined by the trap, the trapped particle localization behavior can be controlled via adjusting optical field parameters in the α_1 term.

As mentioned above, the effective potential can be represented as a superposition of an average kinetic energy of fast oscillation (q-depended term) and the potential energy of the dynamical system (α-terms) [44,45]. Thus, the effective potential is given by

$$U_{\text{eff}} = \frac{q^2}{4} \left[\left(\frac{\partial f_V}{\partial \tilde{x}} \right)^2 + \left(\frac{\partial f_V}{\partial \tilde{y}} \right)^2 + \left(\frac{\partial f_V}{\partial \tilde{z}} \right)^2 \right] - \alpha \tilde{z}. \tag{A6}$$

The effective potential distribution (A6) depends on the following: the charged particle parameters, such as mass m, size r and charge e; the trap's RF field parameters, such as voltage amplitude V and frequency ω. The distribution of the effective potential for

differently sized microparticles localized at various RF voltages and frequencies is shown in Figure A1. Column (a) represents effective potential maps for particles with 2, 3 and 5 μm at fixed RF voltage and frequency. Column (b) represents effective potential maps for RF voltages 2000, 3000 and 5000 V at fixed RF frequency and particle size. Column (c) represents effective potential maps for RF frequencies 50, 100 and 150 Hz at fixed RF voltage and particle size. As can be seen, the DW regime for the proposed electrode geometry is realised only for a specific relation in the varied parameters. Notably, effective potential minima coordinates, marked with red asterisks, strongly depend on all the varied parameters. The physical values of r and ω define the α parameter in Equation (A5), while the physical values of V and ω define the q parameter. To analyze conditions for DW and SW effective potential formation in a general form, we calculated the number of potential minima for different $\alpha - q$ sets in accordance with Equation (A6). Therefore, according to the $\alpha - q$ relation, the effective potential map can have a different number of stable equilibrium points . It should be noted that all the system parameters are explicitly included in α and q parameters. Thus, any variation of these individual parameters can be taken into account as α and q parameter variation.
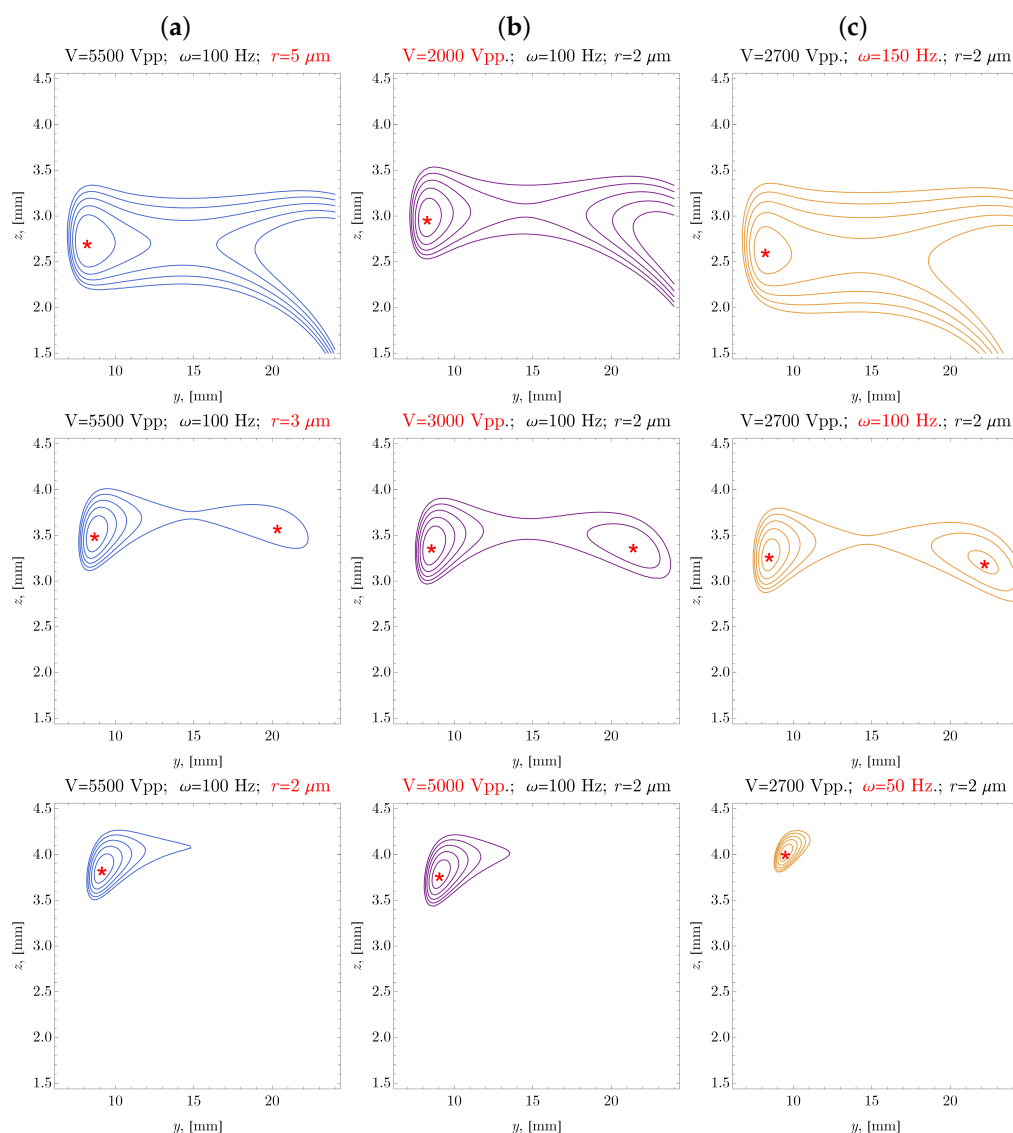

Figure A1. Evolution of effective potential cross sections at $x = 0$ for the case of $\alpha = \alpha_0$: (**a**)—as particle radius r changes; (**b**)—as voltage V changes; (**c**)—as frequency ω changes. Asterisk indicates the potential minima coordinates.

Figure A2 shows the dependence of the number of effective potential minima in coordinates α,q according to the numerical simulation (A5): 0 (unstable), 1 (single-well (SW) regime, Figure 3b) or 2 (double-well (DW) regime, Figure 3a). In Figure A2, the SW regime is marked in blue, DW is marked in green, and the unstable regime is marked in red.

Since α describes the superposition of all the force projections on the OZ-axis, the numerical value of α shows the trapped particle localization behavior, and three general cases are possible. First, a common case where $\alpha_0 > \alpha_1$, which means that the particle's gravitational force is much greater than the light scattering force. Second, a case where $\alpha_0 = \alpha_1$, which implies exact gravity compensation. Third, a case where $\alpha_0 < \alpha_1$, when the light scattering force exceeds the particle's gravity. Therefore, the DW regime is only possible in the first case with uncompensated particle gravitational force (the green zones in Figure A2). For compensation or overcompensation of the particle's gravity the SW regime is only possible (the blue zones in Figure A2).
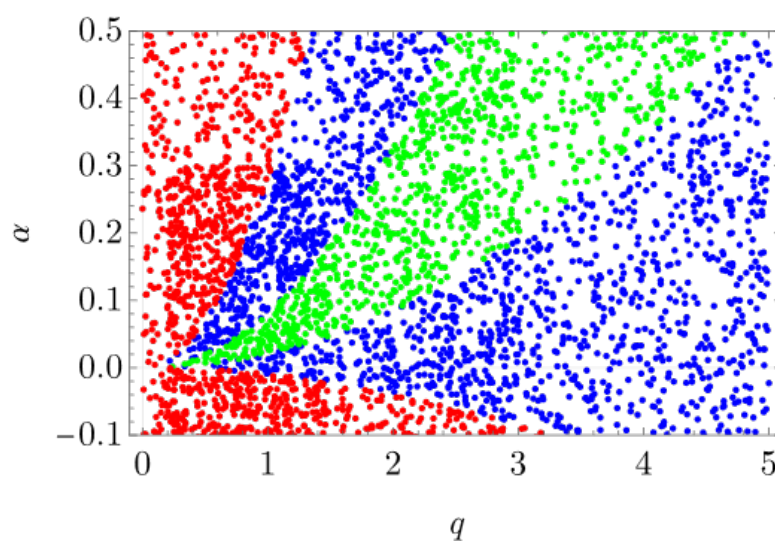

Figure A2. Localization regimes map in surface ITO trap: SW regime is marked in blue, DW is marked in green, unstable is marked in red.

References

1. Paul, W. Electromagnetic traps for charged and neutral particles (Nobel lecture). *Angew. Chem. Int. Ed. Engl.* **1990**, *29*, 739–748. [CrossRef]
2. Kajita, M. *Ion Traps: A Gentle Introduction*; IOP Publishing: Bristol, UK, 2022.
3. Mihalcea, B.M.; Giurgiu, L.C.; Stan, C.; Vişan, G.T.; Ganciu, M.; Filinov, V.; Lapitsky, D.; Deputatova, L.; Syrovatka, R. Multipole electrodynamic ion trap geometries for microparticle confinement under standard ambient temperature and pressure conditions. *J. Appl. Phys.* **2016**, *119*, 114303. [CrossRef]
4. Nolting, D.; Malek, R.; Makarov, A. Ion traps in modern mass spectrometry. *Mass Spectrom. Rev.* **2019**, *38*, 150–168. [CrossRef]
5. Guo, Q.; Gao, L.; Zhai, Y.; Xu, W. Recent developments of miniature ion trap mass spectrometers. *Chin. Chem. Lett.* **2018**, *29*, 1578–1584. [CrossRef]
6. Häffner, H.; Roos, C.F.; Blatt, R. Quantum computing with trapped ions. *Phys. Rep.* **2008**, *469*, 155–203. [CrossRef]
7. Monroe, C.; Kim, J. Scaling the ion trap quantum processor. *Science* **2013**, *339*, 1164–1169. [CrossRef]
8. Nop, G.N.; Paudyal, D.; Smith, J.D. Ytterbium ion trap quantum computing: The current state-of-the-art. *AVS Quantum Sci.* **2021**, *3*, 044101. [CrossRef]
9. Noel, C.; Kozhanov, A.; Cetina, M.; Monroe, C. Trapped ion quantum computers: Challenges and opportunities. In Proceedings of the APS March Meeting 2023, Las Vegas, NV, USA, 5–10 March 2023.
10. Ghosh, I.; Saxena, V.; Krishnamachari, A. Study of Plasma Distribution Function in a Paul Trap using Palette Mapped 3D Plots. In Proceedings of the 2022 IEEE International Conference of Electron Devices Society Kolkata Chapter (EDKCON), Kolkata, India, 26–27 November 2022; IEEE: Piscataway, NJ, USA, 2022; pp. 312–318.
11. Deputatova, L.; Syrovatka, R.; Vasilyak, L.; Filinov, V.; Lapitsky, D.; Vladimirov, V.; Pecherkin, V.Y. Linear electrodynamic trap as a tool for cleaning dusty surfaces. *Contrib. Plasma Phys.* **2019**, *59*, 340–344. [CrossRef]
12. Rybin, V.; Rudyi, S.; Rozhdestvensky, Y. Nano-and microparticle Nonlinear Damping Identification in quadrupole trap. *Int. J. Non-Linear Mech.* **2022**, *147*, 104227. [CrossRef]

13. Xiong, C.; Liu, H.; Liu, C.; Xue, J.; Zhan, L.; Nie, Z. Mass, size, and density measurements of microparticles in a quadrupole ion trap. *Anal. Chem.* **2019**, *91*, 13508–13513. [CrossRef]

14. Farr, A.; Allen, C.; Hilleke, R.; Clark, R. Fluorescent Quantum-Sized Carbon Dots Isolated in an rf Paul Trap. In Proceedings of the APS March Meeting Abstracts, Baltimore, MD, USA, 18–22 March 2013; Volume 2013, pp. 1–114.

15. Nemova, G. Laser cooling and trapping of rare-earth-doped particles. *Appl. Sci.* **2022**, *12*, 3777. [CrossRef]

16. Howder, C.R.; Long, B.A.; Bell, D.M.; Furakawa, K.H.; Johnson, R.C.; Fang, Z.; Anderson, S.L. Photoluminescence of charged CdSe/ZnS quantum dots in the gas phase: Effects of charge and heating on absorption and emission probabilities. *ACS Nano* **2014**, *8*, 12534–12548. [CrossRef]

17. March, R.E. Quadrupole ion traps. *Mass Spectrom. Rev.* **2009**, *28*, 961–989. [CrossRef]

18. Fernandez-Gonzalvo, X.; Keller, M. A fully fiber-integrated ion trap for portable quantum technologies. *Sci. Rep.* **2023**, *13*, 523. [CrossRef]

19. Eltony, A.M.; Wang, S.X.; Akselrod, G.M.; Herskind, P.F.; Chuang, I.L. Transparent ion trap with integrated photodetector. *Appl. Phys. Lett.* **2013**, *102*, 054106. [CrossRef]

20. Stockett, M.H.; Houmøller, J.; Støchkel, K.; Svendsen, A.; Brøndsted Nielsen, S. A cylindrical quadrupole ion trap in combination with an electrospray ion source for gas-phase luminescence and absorption spectroscopy. *Rev. Sci. Instrum.* **2016**, *87*, 053103. [CrossRef]

21. Araneda, G.; Cerchiari, G.; Higginbottom, D.B.; Holz, P.C.; Lakhmanskiy, K.; Obšil, P.; Colombe, Y.; Blatt, R. The Panopticon device: An integrated Paul-trap–hemispherical mirror system for quantum optics. *Rev. Sci. Instrum.* **2020**, *91*, 113201. [CrossRef]

22. Torres, I.; Fernández, S.; Fernández-Vallejo, M.; Arnedo, I.; Gandía, J.J. Graphene-based electrodes for silicon heterojunction solar cell technology. *Materials* **2021**, *14*, 4833. [CrossRef]

23. Salih, E.Y.; Ramizy, A.; Aldaghri, O.; Mohd Sabri, M.F.; Madkhali, N.; Alinad, T.; Ibnaouf, K.H.; Eisa, M.H. In-depth optical analysis of Zn (Al) O mixed metal oxide film-based Zn/Al-layered double hydroxide for TCO application. *Crystals* **2022**, *12*, 79. [CrossRef]

24. Cirocka, A.; Zarzeczańska, D.; Wcisło, A. Good Choice of Electrode Material as the Key to Creating Electrochemical Sensors—Characteristics of Carbon Materials and Transparent Conductive Oxides (TCO). *Materials* **2021**, *14*, 4743. [CrossRef]

25. Ji, C.; Liu, D.; Zhang, C.; Jay Guo, L. Ultrathin-metal-film-based transparent electrodes with relative transmittance surpassing 100%. *Nat. Commun.* **2020**, *11*, 3367. [CrossRef] [PubMed]

26. Kurdesau, F.; Khripunov, G.; Da Cunha, A.; Kaelin, M.; Tiwari, A. Comparative study of ITO layers deposited by DC and RF magnetron sputtering at room temperature. *J. Non-Cryst. Solids* **2006**, *352*, 1466–1470. [CrossRef]

27. Tuna, O.; Selamet, Y.; Aygun, G.; Ozyuzer, L. High quality ITO thin films grown by dc and RF sputtering without oxygen. *J. Phys. D Appl. Phys.* **2010**, *43*, 055402. [CrossRef]

28. Kosarian, A.; Shakiba, M.; Farshidi, E. Role of sputtering power on the microstructural and electro-optical properties of ITO thin films deposited using DC sputtering technique. *IEEJ Trans. Electr. Electron. Eng.* **2018**, *13*, 27–31. [CrossRef]

29. Amalathas, A.P.; Alkaisi, M.M. Effects of film thickness and sputtering power on properties of ITO thin films deposited by RF magnetron sputtering without oxygen. *J. Mater. Sci. Mater. Electron.* **2016**, *27*, 11064–11071. [CrossRef]

30. Cruz, L.; Legnani, C.; Matoso, I.; Ferreira, C.; Moutinho, H. Influence of pressure and annealing on the microstructural and electro-optical properties of RF magnetron sputtered ITO thin films. *Mater. Res. Bull.* **2004**, *39*, 993–1003. [CrossRef]

31. Amosova, L. Electrooptical properties and structural features of amorphous ITO. *Semiconductors* **2015**, *49*, 414–418. [CrossRef]

32. Amosova, L.; Isaev, M. Deposition of transparent indium tin oxide electrodes by magnetron sputtering of a metallic target on a cold substrate. *Tech. Phys.* **2014**, *59*, 1545–1549. [CrossRef]

33. Konshina, E.; Shcherbinin, D.; Kurochkina, M. Comparison of the properties of nematic liquid crystals doped with TiO_2 and CdSe/ZnS nanoparticles. *J. Mol. Liq.* **2018**, *267*, 308–314. [CrossRef]

34. Zhang, X.; Zeng, Q.; Xiong, Y.; Ji, T.; Wang, C.; Shen, X.; Lu, M.; Wang, H.; Wen, S.; Zhang, Y.; et al. Energy level modification with carbon dot interlayers enables efficient perovskite solar cells and quantum dot based light-emitting diodes. *Adv. Funct. Mater.* **2020**, *30*, 1910530. [CrossRef]

35. Almaev, A.V.; Kopyev, V.V.; Novikov, V.A.; Chikiryaka, A.V.; Yakovlev, N.N.; Usseinov, A.B.; Karipbayev, Z.T.; Akilbekov, A.T.; Koishybayeva, Z.K.; Popov, A.I. ITO Thin Films for Low-Resistance Gas Sensors. *Materials* **2022**, *16*, 342. [CrossRef]

36. Deng, J.; Zhang, L.; Hui, L.; Jin, X.; Ma, B. Indium tin oxide thin-film thermocouple probe based on sapphire microrod. *Sensors* **2020**, *20*, 1289. [CrossRef]

37. Kokorina, O.O.; Rybin, V.V.; Rudyi, S.S.; Rozhdestvensky, Y.V. Double-well effective potential in a linear Paul trap with end-cap electrodes. In Proceedings of the Quantum Nanophotonic Materials, Devices, and Systems 2021, International Society for Optics and Photonics, San Diego, CA, USA, 1 August 2021; Volume 11806, p. 118060U.

38. Wang, X.-Y.; Ren, Y.; Hong, Y.; Huang, Q.; Chen, Z.-G.; Yuan, L.-Y.; Huang, Z.-X.; Li, M.; Zhou, Z. Design and Simulation of a Double Potential Well Flat Ion Trap. *J. Chin. Mass Spectrom. Soc.* **2023**, *44*, 34.

39. Malek, R.; Wanczek, K. Trapping and excitation of ions in a double well potential. *Rapid Commun. Mass Spectrom.* **1997**, *11*, 1616–1618. [CrossRef]

40. Tanaka, U.; Suzuki, K.; Ibaraki, Y.; Urabe, S. Design of a surface electrode trap for parallel ion strings. *J. Phys. B At. Mol. Opt. Phys.* **2014**, *47*, 035301. [CrossRef]

41. Tao, J.; Likforman, J.P.; Zhao, P.; Li, H.Y.; Henner, T.; Lim, Y.D.; Seit, W.W.; Guidoni, L.; Tan, C.S. Large-Scale Fabrication of Surface Ion Traps on a 300 mm Glass Wafer. *Phys. Status Solidi* **2021**, *258*, 2000589. [CrossRef]
42. Kurshanov, D.A.; Khavlyuk, P.D.; Baranov, M.A.; Dubavik, A.; Rybin, A.V.; Fedorov, A.V.; Baranov, A.V. Magneto-fluorescent hybrid sensor CaCO3-Fe3O4-AgInS2/ZnS for the detection of heavy metal ions in aqueous media. *Materials* **2020**, *13*, 4373. [CrossRef]
43. Peng, W.P.; Lin, H.C.; Chu, M.L.; Chang, H.C.; Lin, H.H.; Yu, A.L.; Chen, C.H. Charge monitoring cell mass spectrometry. *Anal. Chem.* **2008**, *80*, 2524–2530. [CrossRef]
44. Gerlich, D. Inhomogeneous RF fields: A versatile tool for the study of processes with slow ions. *State-Sel. State-Ion-Mol. React. Dyn. Part 1 Exp.* **1992**, *82*, 1–176.
45. Rudyi, S.S.; Vovk, T.A.; Rozhdestvensky, Y.V. Features of the effective potential formed by multipole ion trap. *J. Phys. B At. Mol. Opt. Phys.* **2019**, *52*, 095001. [CrossRef]
46. Lechner, K. *Classical Electrodynamics*; Springer: Cham, Switzerland, 2018.
47. Abbas, M.; Craven, P.; Spann, J.; Witherow, W.; West, E.; Gallagher, D.; Adrian, M.; Fishman, G.; Tankosic, D.; LeClair, A.; et al. Radiation pressure measurements on micron-size individual dust grains. *J. Geophys. Res. Space Phys.* **2003**, *108*, A6. [CrossRef]